



# Complex Catalogue of High Speed Streams Associated with Geomagnetic Storms During Solar Cycle 24

Diana Besliu-Ionescu<sup>1,2</sup> · Georgeta Maris Muntean<sup>2</sup> · Venera Dobrica<sup>2</sup>

Received: 29 December 2021 / Accepted: 5 May 2022 / Published online: 30 May 2022  
© The Author(s), under exclusive licence to Springer Nature B.V. 2022

## Abstract

A complex catalogue of high speed streams produced by coronal holes and their effects in the terrestrial magnetosphere – the so-called geomagnetic storms – for Solar Cycle 24 (2009 to 2019) is presented here. This catalogue is structured in three parts describing the high-speed stream characteristics, the interplanetary magnetic field state, and the properties of the associated geomagnetic storms. The catalogue is available online at <http://www.geodin.ro/varsiti/>.

**Keywords** Solar wind · Geomagnetic disturbances · Coronal holes

## 1. Introduction

High-speed streams (HSSs) in the solar wind are an important physical driver of space weather. Along with other solar-driven phenomena, they may seriously impact various aspects of our increasingly sophisticated technological lives.

Solar wind (SW) is “the medium” through which all solar disturbances propagate towards the Earth and throughout the solar system. Amongst the most important observations of the solar wind, data from Ulysses (Phillips et al., 1995) have shown a latitudinal dependence of the solar wind speed: solar wind originating from the poles is fast ( $500\text{--}800\text{ km s}^{-1}$ ), whereas its speed at lower latitudes tends towards  $300\text{--}400\text{ km s}^{-1}$ . Practically, there are two components of the solar wind: a slow solar wind and a fast (rapid) one. The slow solar wind is characterized by velocities of about  $300\text{--}350\text{ km s}^{-1}$ , temperatures of  $1.4\text{--}1.6 \times 10^6\text{ K}$ , and a composition similar to that of the solar corona. The fast solar wind has a

---

✉ D. Besliu-Ionescu  
[diana.ionescu@astro.ro](mailto:diana.ionescu@astro.ro)

G. Maris Muntean  
[gmastro05@yahoo.com](mailto:gmastro05@yahoo.com)

V. Dobrica  
[venera@geodin.ro](mailto:venera@geodin.ro)

<sup>1</sup> Astronomical Institute of the Romanian Academy, Str. Cutitul de argint, Nr. 5, Sector 4, Bucharest 040557, Romania

<sup>2</sup> Institute of Geodynamics of the Romanian Academy, Str. J.L. Calderon, Nr. 19-21, Sector 2, Bucharest 020032, Romania

typical speed of about  $500\text{--}750\text{ km s}^{-1}$ , temperatures of  $8 \times 10^5\text{ K}$ , and it resembles the composition of the Sun's photosphere.

Coronal holes (CHs), the important sources of the fast solar wind, tend to appear in regions near the Sun's poles. CHs are also sources of the slow wind, which could emerge from the bordering divergent regions of the holes. The fast wind from such CHs catches up with downstream slow solar wind, forming co-rotating interaction regions (CIRs), followed by an HSS. CHs can also appear at lower solar latitudes and near the solar equator, either as discrete regions or as long (even trans-equatorial) extensions from a polar coronal hole. Such extended CHs can appear during all phases of the 11-year cycle, but they are more noticeable during the descending and minimum phases.

Our catalogue for Solar Cycle 24 (SC24) considers only HSSs generated by coronal holes. These HSSs are recurrent, co-rotating streams with an apparent tendency to occur every 27 days. There are also non-recurrent HSSs produced by certain eruptive solar phenomena such as flares, coronal mass ejections (CMEs), sudden disappearing filaments, or eruptive prominences. Time variation of the HSS features and their occurrence rate show significant differences in comparison with the well-known 11-year solar cycle.

Generally speaking, a high-speed stream is characterized by a large increase in the solar wind speed lasting for several days. Over the years, a number of HSSs definitions were given by different authors using the increase in speed and the duration of these streams (see Lindblad and Lundstedt, 1981, and the references herein).

Based on some imposed values of growth in plasma speed from one day to the next one, and on the maximum speed of the streams, different authors have set up HSS catalogues for more than five 11-year solar cycles. Such catalogues are extremely valuable as they help researchers understand the solar wind state close to the Earth from the point of view of the speed state at a given moment. We mention here the important catalogues covering Solar Cycles (SCs) 20–23 performed by the Swedish team (Lindblad and Lundstedt, 1981, 1983; Lindblad, Lundstedt, and Larsson, 1989) and the Greek team (Mavromichalaki, Vassilaki, and Marmatsouri, 1988; Mavromichalaki and Vassilaki, 1998), as well as one Indian catalogue (Gupta and Badruddin, 2010), along with our team catalogue (Maris and Maris, 2012). Using the same definition as the one adopted by the Swedish team, we selected as a high-speed stream a solar wind flow having a jump in speed of more than  $100\text{ km s}^{-1}$  from one day to the next and lasting for at least two days.

HSS catalogues for SC24 (whole cycle, or part of it) were set up by Gerontidou, Mavromichalaki, and Daglis (2018), Muntean, Besliu-Ionescu, and Dobrica (2018), and Grandin, Aikio, and Kozlovsky (2019).

The study of Grandin, Aikio, and Kozlovsky (2019) focused on finding the geoeffective stream interaction regions (SIRs)/HSSs. They used as a first criterion for the selection of SIRs the time derivative of the magnetic field ( $B$ ) with an empirically set threshold of  $0.6\text{ nT h}^{-1}$  (with the time resolution of the data being 1 h). Then, the criterion related to the solar wind speed came in second place. Their threshold set empirically for the SW speed is  $450\text{ km s}^{-1}$ , with an average slope between consecutive days greater than  $30\text{ km s}^{-1}$ . Grandin, Aikio, and Kozlovsky (2019) also imposed a  $500\text{ km s}^{-1}$  threshold to be reached within the first three days of the stream. They also introduced a factor for determining identical currents or superimposed ones that kept only SIR/HSS event starting times separated by at least 3 days.

Our catalogue intends to distinctively show HSS basic properties, their sources, parameters of the interplanetary magnetic field, and various properties related to the associated geomagnetic storms. In the study by Zhang et al. (2007), the authors showed that the solar sources of 88 major geomagnetic storms consisted of CMEs (89%) and CIRs (11%).

In order to define geomagnetic storms (GSs), we used the Gonzalez et al. (1994) criterion that specifies their intensities by the Dst minimum value, such that a minor storm is defined by a  $-50 < \text{Dst}_{\min} \leq -30$  nT, a moderate storm by  $-100 < \text{Dst}_{\min} \leq -50$  nT, and an intense storm by  $\text{Dst}_{\min} \leq -100$  nT.

This article is structured as follows: a section about the HSS detection method used for identifying the HSSs (Section 2); a section that describes the catalogue (Section 3) with sub-sections for the HSS features (Section 3.1), one for interplanetary conditions (Section 3.2), and one describing the association of HSSs with geomagnetic storms (Section 3.3). They are followed by a section that summarizes the statistics of the detected HSSs (Section 4) and a section presenting two selected events: an HSS with an associated GS and one that had no GS (Section 5). The article ends with a summary (Section 6).

## 2. HSS Detection Method

It is known that geomagnetic activity and other associated phenomena are influenced more by the variation of the solar wind stream speed,  $dV/dt$ , rather than by the absolute value of the speed of the solar wind particles (Lindblad and Lundstedt, 1981, and references therein). For this reason, in the attempt to define HSSs, the criterion of the SW speed variation rather than its absolute value has been used. Consequently, we chose the same selection procedure for the streams as the one adopted by the Swedish team (e.g. Lindblad and Lundstedt, 1981, 1983). Moreover, this selection method allows a more accurate determination of the HSS start and end in comparison with that used by Mavromichalaki, Vassilaki, and Marmatsouri (1988).

In order to identify the HSS events, software in the IDL programming language was developed. In the first step, the software reads the input data (hourly SW plasma speed values) from the source data files and fills in the gaps in the data series using linear interpolation. For our dataset, the gaps are usually about 1–6 h and extremely rarely longer than 24 h. The input data is available online in the OMNI database – <https://omniweb.gsfc.nasa.gov/form/dx1.html> (King and Papitashvili, 2005). The chosen input data consist of the Bartels rotation number, the SW plasma temperature (K), SW proton density ( $\text{N cm}^{-3}$ ), SW plasma speed ( $\text{km s}^{-1}$ ).

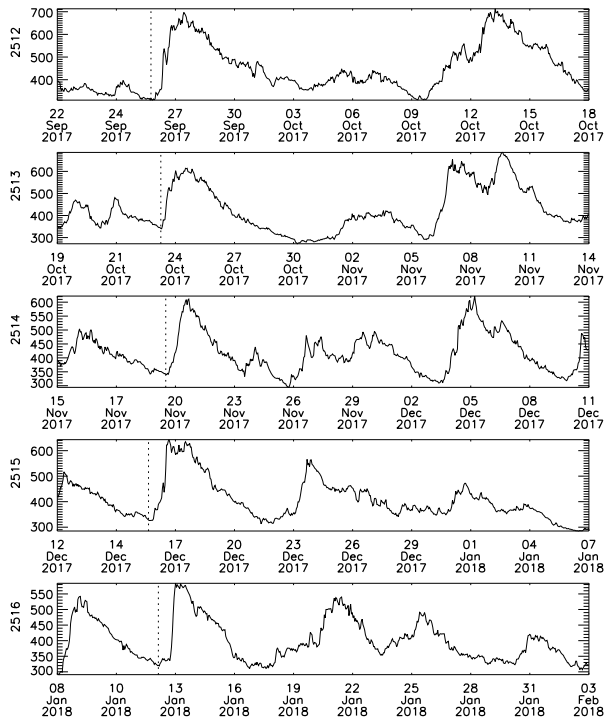
After the initial data input, the 3-h mean values were computed. Thus, for each day represented by the data, there are eight 3-h values. The motivation for using 3-h values is based on the availability of the Kp index data, which is computed as a 3-hour range index. Kp is a geomagnetic index characterizing the magnitude of the geomagnetic storm. It was initially used for the association between HSSs and GSs.

In the second step, the software computes the maximum ( $V_{\max}$ ) and minimum ( $V_{\min}$ ) values of the 3-h speed for each daily set of eight values, as well as the corresponding 3-h time, which takes values from 1 to 8. Then, the algorithm implemented by the software looks for and identifies the speed increase for two consecutive days described by:

$$V_{\max \text{ next}} - V_{\min} > 100 \text{ km s}^{-1}. \quad (1)$$

For an identified event, the 3-h time corresponding to  $V_{\min}$  represents the start time  $t_0$  of the event, whereas  $V_{\min}$  represents the prestream minimum speed value  $V_0$  of the event;  $V_{\max \text{ next}}$  (maximum velocity of the next day) becomes  $V_1$ . To complete the identification of the HSS event that meets the selection conditions, the algorithm continues with the identification of the maximum speed  $V_{\max}$ , which could happen later on and could be even greater

**Figure 1** SW plasma speed plotted over five Bartels rotations showing some recurrent streams. The vertical bar indicates the beginning of one recurrent stream in successive rotations. The numbers to the left of vertical axes correspond to the Bartels rotations, and the units of these axes are  $\text{km s}^{-1}$ .



than  $V_1$  or coincide with the maximum speed of the following day of the event,  $V_1$ . Then, the algorithm continues with the identification of the end time of the event, when the speed decreases to (or near to) the  $V_0$  value of the beginning of the event. If a new increase greater than  $100 \text{ km s}^{-1}$  appeared before the fall under the initial speed value  $V_0$ , it is considered a new HSS event start, so that the starting value of the new stream is taken as the end of the previous one. Knowing the 3-h values for the beginning and the end of the HSS event, the algorithm computes the duration ( $d$ ) of the event in days. It also computes the maximum increase (gradient) of the speed,  $\Delta V_{\text{max}}$  (written as  $\Delta VM$  in the catalogue and as  $\Delta V_{\text{max}}$  in this text), as the difference between  $V_{\text{max}}$  and  $V_0$ .

The output file lists numbered HSSs detected along with their start time, duration, initial and maximum speed values, and speed gradients. The identification of the solar corona phenomenon, responsible for emitting a high-speed particle stream (solar source), is made using the criteria described below. The first criterion is the analysis of the speed and density profiles for the solar wind stream. With regard to the streams emitted by CHs, a sudden increase in the particle density of the stream is observed before the speed-increase phase.

The second criterion consists of identifying the co-rotational behavior of the coronal-hole HSS. That means that the stream is found in the records of the following Bartels rotation, and it is repeated numerous times in subsequent rotations because CHs are persistent, long-lasting regions in the solar corona.

Figure 1 shows several streams that have been identified in five different Bartels rotations during late 2017 and the beginning of 2018. The vertical bar indicates the beginning of one recurrent stream in successive rotations.

We identified the CH sources in the list prepared by Jan Alvestad, available online at [http://www.soleno.info/solar/coronal\\_holes.html](http://www.soleno.info/solar/coronal_holes.html). We also used the CH data from Solar and

**Figure 2** SW plasma speed and density plot for the complex HSS of 25 August 2018.

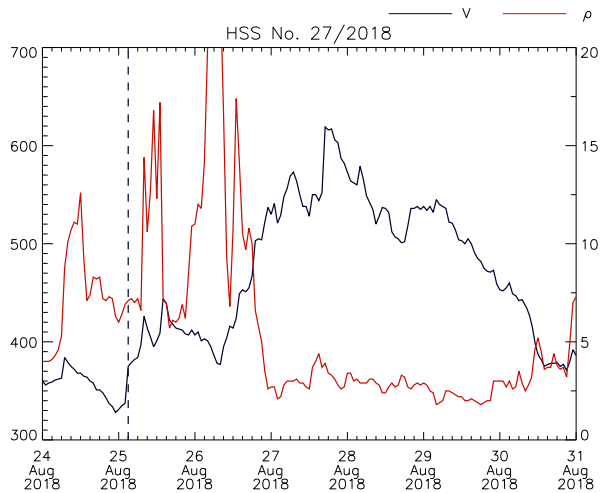


**Table 1** The parameters of HSS Nr 27 from 25 August 2018 as output from the software.

Nr	Year	Mon	Day	3H	$V_0$	$V_1$	$dt1$	$V_{max}$	$Dur$	$DV1$	$DVM$
27	2018	8	25	1	334.3	521	15	613	8.4	186.7	278.7

Heliospheric Observatory (SOHO: Domingo, Fleck, and Poland, 1995) and the Solar Dynamics Observatory (SDO: Pesnell, Thompson, and Chamberlin, 2012) to identify the CH sources that were not included in Alvestad's list.

Finally, a careful analysis of the plots representing the time evolution of the SW speed and density was necessary for correctly estimating the start and end times of the complex HSS events. The output file was also validated by a human operator because of possible superposition of HSSs emitted by a coronal hole with other eruptive phenomena in the SW. We note that our HSS catalogue contains eight HSSs that had a complex source consisting of CHs and some contribution from ICMEs. We have included these phenomena in the catalogue because it is difficult to decide about each source contribution to the HSS registered by space missions in the Lagrangian point L1. Next, we illustrate one of these complex HSSs. In Figure 2, the SW speed and density for the 25 August 2018 HSS (HSS Nr 27 in 2018 table, online catalogue) are presented. Our algorithm associated this HSS with the parameters listed in Table 1.

The main solar source of this HSS was a northern CH visible and marked in Figure 3 (left panel). At the onset of the HSS, an ICME particle flux produced by a faint and slow-moving CME, which left the Sun on 21 August, was recorded. The combined effect of CH and ICME particle flux triggered a strong geomagnetic storm on 26 August ( $Dst_{min} = -174$  nT). The HSS continued and was again fuelled by a new particle flux given by a widely spread trans-equatorial CH (Figure 3, right panel).

We have chosen two examples to illustrate how the validation was done. Figure 4 shows the SW plasma speed and density for the complex HSS events of February and June 2016. From 14 to 25 February 2016 (left frame), the software output listed two streams marked by dashed vertical lines with full data description included in the first two rows of Table 2. Upon careful examination of these profiles and the evolution of the triggering CH as illustrated in

**Figure 3** SDO/AIA 193 Å illustrating CH sources for the 24 and 27 August 2018 HSS. ©spaceweather.com.

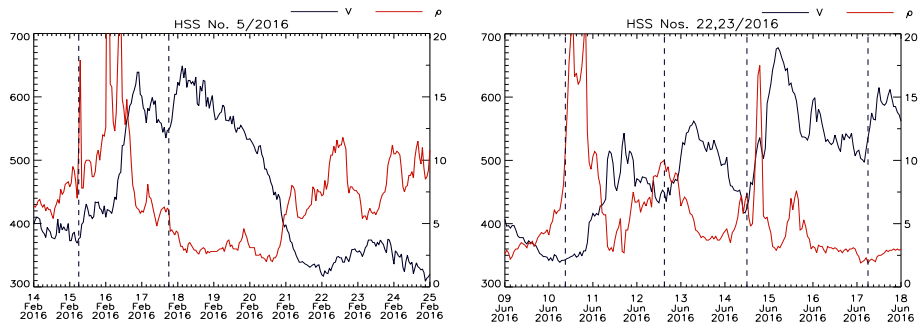
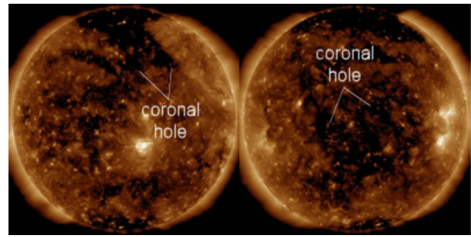


**Figure 4** SW plasma speed (black) and density (red) for the selected validation examples.

**Table 2** Examples of combined streams before and after validation for the HSSs in February and June of 2016. The first rows are the output from the algorithm and the rows highlighted in gray are the validated results.

Nr	Year	Mon	Day	3H	$V_0$	$V_1$	$dt1$	$V_{max}$	$Dur$	$DV1$	$DVM$
5	2016	2	15	2	375.0	624.3	14	624.3	2.5	249.3	249.3
6	2016	2	17	6	542.3	642.7	4	642.7	2.2	100.4	100.4
5	2016	2	15	2	375	624.3	14	642.7	6	249.3	267.7
25	2016	6	10	3	340.7	516.0	11	516.0	2.2	175.3	175.3
26	2016	6	12	5	443.0	556.3	6	556.3	1.9	113.3	113.3
27	2016	6	14	4	424.3	668.7	6	668.7	2.8	244.4	244.4
28	2016	6	17	2	508.0	614.7	14	614.7	2.6	106.7	106.7
22	2016	6	10	3	340.7	516	11	556.3	4.1	175.3	216.6
23	2016	6	14	4	424.3	668.7	6	668.7	6.7	244.4	244.4

Figure 5, we merged the two streams into one highlighted in gray in Table 2 because the two HSSs had the same source (the southern CH marked in Figure 5) with a complex structure. Another reason for merging the two HSSs was the particle speed during the total duration.

From 10 to 18 June 2016, the software output lists four different streams, whose starts are marked by vertical dashed lines (Figure 4, right panel). The detailed data are listed in rows from 4 to 7 in Table 2. These were confined to two streams (the last two gray rows from Table 2) after analyzing the evolution of the triggering CHs, as seen in Figure 6, because of similar considerations as the previous example.

**Figure 5** SDO/AIA 193 Å illustrating the evolution of the CH sources for 15 and 19 February 2016. ©spaceweather.com.

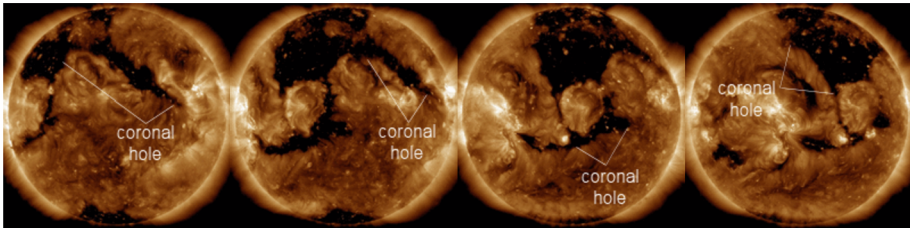
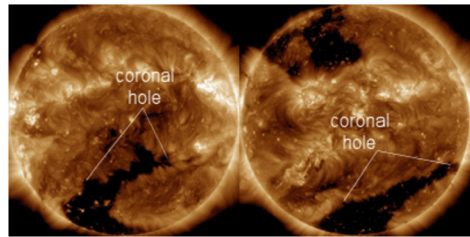


**Figure 6** SDO/AIA 193 Å illustrating the evolution of the CH sources for 10, 12, 14, and 16 June 2016. ©spaceweather.com.

### 3. Catalogue Description

Our catalogue for Solar Cycle 24 (2009–2019) is available at <http://www.geodin.ro/varsiti/>. We mention that the building of the main part of this catalogue (2009–2016) was supported by a VarSITI/SCOSTEP (Variability of the Sun and Its Terrestrial Impact/Scientific Committee on Solar-Terrestrial Physics) grant in 2017. We have also made available the HSS catalogue for SC23 at <http://www.geodin.ro/hss-sc23/>. This catalogue contains data of HSSs from 1996 to 2008 having CHs or an eruptive solar phenomenon (CME, solar flare, active prominences) as their sources.

The present catalogue (for SC24) is structured into three different parts: HSS general parameters, some data on the interplanetary magnetic field (IMF), and some data about geomagnetic storms triggered by the HSS impact on the terrestrial magnetosphere.

From the online tables, we have removed the columns for the Bartels rotation numbers and the day of that rotation, such that the table is easily readable on web browsers. This data can be found at <http://www.srl.caltech.edu/ACE/ASC/DATA/bartels/Bartels2004-2023.pdf>.

#### 3.1. HSS Features

The first part of the catalogue lists the basic parameters of the HSSs. The first column gives the identification number representing the chronological detection of the HSS in the year shown. The next three columns (2–4) show the HSS start time listed as year, month, and day. The fifth column shows a number between 1–8, which represents the  $x$ th 3-hour interval of the day when the HSS started. The sixth and seventh columns show the initial ( $V_0$ ) and maximum ( $V_1$ ) velocities in the second day of the stream ( $\text{km s}^{-1}$ ). The next column lists  $\Delta t_1$  (or  $dt_1$ ), which represents the time interval between  $V_0$  and  $V_1$  (in units of 3-h intervals).

The ninth column shows the maximum ( $V_{\text{max}}$ ) speed (in  $\text{km s}^{-1}$ ) of the stream reached during its detection. The next column shows the duration (in days) of the HSS. The eleventh



and twelfth columns list the gradient of the plasma speed (in  $\text{km s}^{-1}$ ) between the two consecutive days:  $\Delta V_1 = V_1 - V_0$ , and the maximum gradient of the HSS plasma velocity,  $\Delta V_{\text{max}} = V_{\text{max}} - V_0$ .

The thirteenth column shows the importance of the stream defined as  $I = \Delta V_{\text{max}} \times d$ , ( $d$  being the duration of the HSS) (Sykora, 1992; Maris and Maris, 2005). This column is the last one in the catalogue showing the basic properties (features) of the detected streams. The next column (fourteenth) of the catalogue points out the sources of the HSS that were validated by a human operator. They were mainly identified from [http://www.solen.info/solar/coronal\\_holes.html](http://www.solen.info/solar/coronal_holes.html) or <http://spaceweather.com/>. The first link represents a report that has been prepared by Jan Alvestad based on the analysis of data from whatever sources available at the time the report was prepared. For some HSSs, we did not find the CH sources in this list and identified the CHs in SOHO or SDO images available at <http://spaceweather.com/> (noted by CH\*).

### 3.2. Interplanetary Field

The next part of the catalogue concerns the interplanetary magnetic field (IMF). We have chosen to list in the next column (fifteenth) the dominant polarity of the IMF, which can have positive or negative values. If the HSS passed over or was overlaid on an IMF magnetic boundary, the notation is “+/-” or “-/+”. All the HSS catalogues for SCs 20–23 also list the dominant polarity of the IMF for the duration of streams.

We have also listed the minimum  $B_z$  (the southern IMF component) value that was recorded during the geomagnetic storm and its occurrence time in columns 18 and 19, respectively. Our motivation for including  $B_z$  is that when it takes negative values, reconnection occurs between the IMF and the geomagnetic field, as well as energy transfer from the solar wind into the terrestrial magnetosphere that drives the occurrence of geomagnetic storms (Cerrato, Saiz, and Cid, 2012). These data, shown after the Dst index and presented in the next subsection, support our analysis of the geomagnetic storm conditions.

### 3.3. Geomagnetic Storm Features

Unlike other catalogues (Mavromichalaki and Vassilaki, 1998; Gerontidou, Mavromichalaki, and Daglis, 2018; Grandin, Aikio, and Kozlovsky, 2019), the information about GSs is more detailed and is available online at <http://www.geodin.ro/varsiti/>.

We chose to describe the intensity of a geomagnetic storm using the Dst index, which is calculated using data from four observatories situated at low latitudes (Sugiura and coworkers, Resolution 2, p. 123, in IAGA Bulletin 27, 1969). This index decreases with the enhancement of the ring current, thus more accurately describing the GS. For the duration of the HSSs, we have analyzed the temporal profile of the Dst index and identified the GSs. For all these associations, we listed the Dst minimum value along with the time at which this minimum occurred in a single column with the date in the format month, day, and hour (mm:dd:hh).

We also analyzed the IMF southern component evolution during the geomagnetic storm and listed its minimum negative values ( $B_z$ , in nT) registered just before the minimum Dst and its time in the format used for the other columns (mm:dd:hh). However, there are a few events where the minimum  $B_z$  value has been reached after the time of the minimum Dst.

Besides the main phase and the recovery phase, a geomagnetic storm has an “initial phase”. This phase presents a period of enhanced Dst, which sometimes starts after a sudden storm commencement (SSC). In fact, the SSC is the effect of compression of the dayside



magnetosphere by enhanced solar wind pressure. During the initial phase, the  $B_z$  component is oriented primarily northward (Cid, Saiz, and Cerrato, 2012).

Joselyn and Tsurutani (1990) stated that a sharp change of at least 10 nT lasting for at least three minutes, followed by a decrease in Dst below at least  $-50$  nT within 24 h, is called a storm sudden commencement. The SSC data used in this catalogue was retrieved from <http://www.obsebre.es/en/rapid> (data available under Creative Commons Attribution-NonCommercial 4.0 International License). The times at which SSCs were recorded are listed in the twentieth column.

In order to give a better estimate of the GS evolution and characteristics, our catalogue also includes estimated values for the energy deposited in the magnetosphere from the solar wind. These estimates are computed using the Akasofu parameter (Akasofu, 1981), noted by  $\epsilon$  (Equation 2), and an improved version of this equation given by Wang et al. (2014), noted by  $W$  (Equation 3). This improved version of the energy transfer equation was introduced using 240 numerical tests indicating that this energy coupling function gives better correlations than the Akasofu parameter.

$$\epsilon = 10^7 V B^2 l_0^2 \sin^4 \left( \frac{\theta}{2} \right) \text{ [J/s]}, \quad (2)$$

$$W = 3.78 \times 10^7 n_{\text{SW}}^{0.24} V_{\text{SW}}^{1.47} B_T^{0.86} \left( \sin^{2.7} \left( \frac{\theta}{2} \right) + 0.25 \right) \text{ [J/s]}. \quad (3)$$

In the above equations,  $l_0$  is an empirical scaling factor denoting the linear dimension of the “effective cross-sectional area” of the solar wind-magnetosphere (SW-M) interaction, which is usually assumed to be 7 RE (Earth radii),  $\theta$  is the IMF clock angle,  $n_{\text{SW}}$  is the solar wind number density in  $\text{cm}^{-3}$ , and  $B_T = \sqrt{B_x^2 + B_y^2}$  is the transverse magnetic field.

Using these two quantities, we were able to compute the total energy transferred from the SW into the magnetosphere by integrating them during the main phase of the geomagnetic storm:

$$\int_{T_0}^{T_F} \epsilon dt = \Delta W \epsilon \text{ [J]} \quad \text{and} \quad \int_{T_0}^{T_F} W dt = \Delta W \text{ [J]}. \quad (4)$$

These values were calculated for moderate and intense geomagnetic storms ( $\text{Dst} \leq -50$  nT) and are shown in columns 21 and 22.

The main phase of the storm is defined as the interval when Dst is clearly decreasing, considering that for moderate geomagnetic storms, the initial phase can be long and include its initial variations. Generally speaking, one single geomagnetic storm is induced by one HSS. However, there are some events when, during a complex HSS, two or even more (usually minor) geomagnetic storms are registered; in such cases, the parameters of the successive geomagnetic storms appear in successive rows in the catalogue.

Recently many scientists have begun to use the 1-min SYM-H geomagnetic index instead of the classic Dst; both indices are designed to measure the ring current intensity during storms. Although there are some clear differences in the method of derivation and in the number and location of ground geomagnetic stations, the main difference between Dst and SYM-H is the time resolution. Also, the effects of the solar wind dynamic pressure variations are more clearly seen in the SYM-H than in the hourly Dst index. A long-term comparison of the Dst and SYM-H indices, made by Wanliss and Showalter (2006), showed that the difference between hourly Dst and 1-min SYM-H indices should be a few nT in case of small storms and of about several tens of nT for moderate and intense geomagnetic storms.

**Table 3** Annual statistics of HSSs during Solar Cycle 24. The largest value for each row is highlighted in gray.

Year	2009	2010	2011	2012	2013	2014	2015	2016	2017	2018	2019
N <sup>o</sup> HSSs	29	27	36	32	31	26	44	43	39	43	35
N <sup>o</sup> HSSs/mon	2.4	2.5	3.0	2.7	2.6	2.2	3.7	3.6	3.3	3.6	2.9
$V_{\max} > 600 \text{ km s}^{-1}$	0	9	11	10	8	7	16	21	25	13	8
$V_{\max} > 700 \text{ km s}^{-1}$	0	2	3	4	3	2	5	5	7	0	2
$\Delta V_{\max} > 400 \text{ km s}^{-1}$	0	2	0	0	2	1	1	3	1	0	0

The authors recommended using the SYM-H index as “a de facto high resolution Dst index”. Therefore, for the sake of completeness, we added in our catalogue (in the last two columns) the minimum value of SYM-H and its time for geomagnetic storms driven by HSS.

#### 4. HSS Statistics

As stated by Maris and Maris (2012), the HSS catalogue for SC23 contains information on about 599 HSSs: 432 – produced by CH (CH\_HSSs) – and 167 – produced by different eruptive solar events (FG\_HSSs) such as CMEs, solar flares or different eruptive prominences or filaments. The HSS analysis by a frequency index (number of events) can be seen in Table 1 in Maris and Maris (2012). Maris and Maris (2012) noticed that SC23 proved to have high-energetic streams distributed during the entirety of its 13-year duration without considering their solar origin. Two aspects were remarkable: the significant activity on the descending phase (2003 and 2005) and the high level of CH\_HSS activity during the 2006–2008 minimum. Maris and Maris (2012) have also found that in most cases, the time of minimum  $B_z$  precedes the time of the minimum Dst value by two hours. There were only two cases for which this time difference was six hours, two cases for which it was five hours, and only one case when they were simultaneous.

This study focuses on the SC24 catalogue that contains 385 HSSs associated with 282 geomagnetic storms. The data given in the catalogue can be used to analyze HSSs and evaluate their statistics and geoeffectivity during the full solar cycle or during some specific intervals.

There are two classes of parameters (indices) used to analyze solar activity, namely the frequency and importance parameters (Kuklin, 1976). The frequency parameter reflects the frequency of the phenomenon occurrence, but it gives little information about its energy. In turn, the one containing information on the phenomenon importance somehow evaluates its energy. We consider the importance parameter more useful for the HSS analysis.

Firstly, an HSS analysis by a frequency index (number of events) can be done using Table 3 and Figure 7. The total number of HSSs has significant maxima in the 2016–2019 interval, which is on the descending phase of SC24 (Figure 7). There is one more maximum in 2012 just before the first peak of the sunspot number (SSN) in this cycle. The lowest HSS number is found in 2015; the second SSN maximum of SC24 is even higher than the first one. Coronal holes are obviously more developed and persistent during the minimum phase of the solar cycle, but SC24 also proved to develop remarkable HSS activity produced by CHs just before the cycle maximum (in 2011) and during the whole descending phase (2016–2018) (Table 3 and Figure 7). We found that 46% of the detected HSSs were followed by geomagnetic storms. The number of associated geomagnetic storms does not

**Figure 7** Sunspot number plot with number of HSSs (black bars) and associated GSs (red bars).

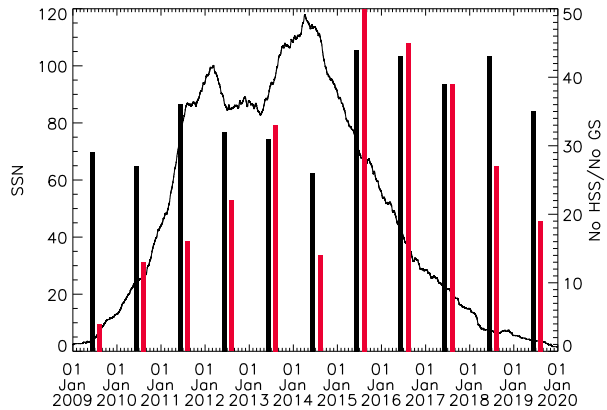
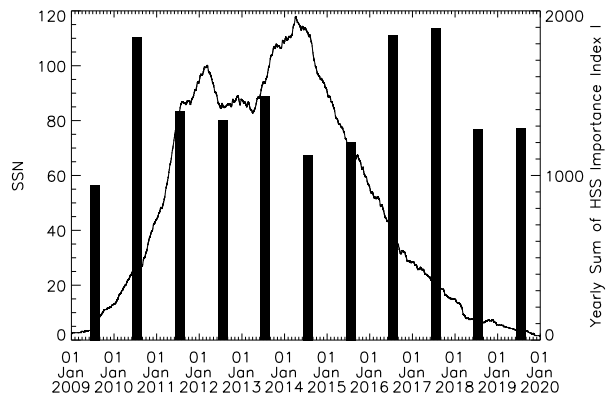


**Figure 8** HSS importance index  $I$  plotted against the smoothed monthly sunspot number.



follow the number of HSSs. Important geomagnetic activity was registered during the descending phase of SC24 (2016–2018). We note a relatively high number of GSs in 2014, during the maximum phase of SC24 (between the two SSN maxima). The red histograms in Figure 7 show the lowest number of GSs in 2009 (minimum phase) and relatively low GS number on the ascending phase (2011–2012), in 2014 (second SSN peak), and also a decreasing geomagnetic activity during the last two years of SC24.

In their analysis, Maris and Maris (2012) have also used the importance index defined in Maris and Maris (2005),  $I = \Delta V_{\max} \times d$ . The HSS index  $I$  includes the gradient of the SW speed as well as the stream duration evaluating somehow the energy of the streams; it can be considered as belonging to the parameters of “importance”. Generally speaking, we can calculate some  $I$  indexes summed over a specific interval of interest, e.g. per month or year. Figure 8 illustrates the yearly distributions of the summed importance indexes (black histograms) superimposed on the smoothed sunspot numbers. Note here that the summed yearly importance of HSSs shows three maxima, two of them during the descending phase (2017–2018) and one in 2011, on the ascending phase. There is a minimum of the index  $I$  in 2014 (during the maximum phase) and at the beginning of the cycle (2009).

Table 3 summarizes some of the HSS main characteristics. Thus, the first row lists the total number of detected HSSs. The second row lists the monthly mean number. The third and fourth rows list the number of HSSs that had their  $V_{\max}$  larger than 600 and 700 km s<sup>-1</sup>,

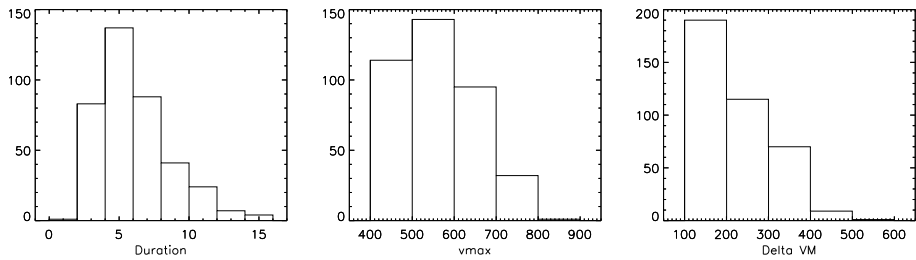


**Figure 9** HSS histograms for their duration,  $V_{\max}$ , and  $\Delta V_{\max}$ .

**Table 4** Statistics of HSSs during each phase of Solar Cycle 24. The highest rates are highlighted in gray.

Phase	Interval	N <sup>o</sup> HSSs	N <sup>o</sup> HSSs/mon.
Part of the Minimum Phase 1	January 2009 – March 2010	34	2.4
Ascending Phase	April 2010 – June 2011	42	2.8
Maximum Phase	July 2011 – March 2015	117	2.7
Descending Phase	April 2015 – July 2017	94	3.4
Part of the Minimum Phase 2	August 2017 – December 2019	98	3.4

respectively. The last row lists the number of HSSs that had the maximum speed jump greater than  $400 \text{ km s}^{-1}$ . In each row, the largest value is highlighted in gray.

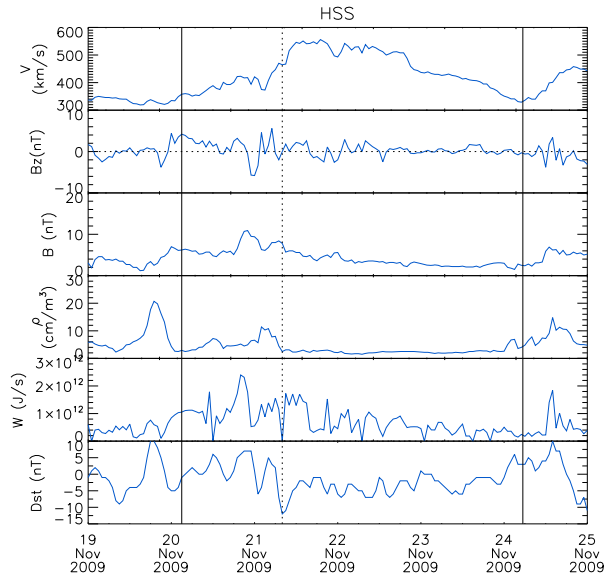
We can observe that the maximum monthly rate of HSSs takes place during the descending phase of Solar Cycles 23 and 24, which is probably due to more complex structured CHs. As the catalogue for SC23 comprises HSSs triggered by CHs and CMEs we cannot clearly compare the two statistics; however, we note a similar behavior – that is, a preference for the descending phase of the cycle.

We studied the HSS distribution considering their duration in two days bins (Figure 9, left panel). According to the HSS definition, their duration has to be more than two days. However, carefully analyzing the 3-h velocity plots, we have considered as HSS some increases in plasma speed higher than  $100 \text{ km s}^{-1}$  that lasted for almost two days, especially if they were isolated, well-defined HSS (Nr. 6 in 2015). The peak of the HSS durations during SC24 is in the 4–6 days interval, and the high majority of the streams lasted for 2–8 days.

The HSS distribution in intervals of  $100 \text{ km s}^{-1}$  of their maximum speed ( $V_{\max}$ , middle panel in Figure 9) presents a maximum number between  $500\text{--}600 \text{ km s}^{-1}$  followed by a significant number of HSSs having  $V_{\max}$  in the  $400\text{--}500 \text{ km s}^{-1}$  interval. These SW speeds ( $400\text{--}600 \text{ km s}^{-1}$ ) correspond to the majority of HSSs during SC24 (59%), while the HSS number with  $V_{\max}$  higher than  $600 \text{ km s}^{-1}$  represents 41% of the total HSSs (see also Table 3). The HSS distribution in  $100 \text{ km s}^{-1}$  intervals of their speed gradient ( $\Delta V_{\max}$ , right panel in Figure 9) shows the maximum number of HSSs have an SW speed gradient in the  $100\text{--}200 \text{ km s}^{-1}$  interval. This interval, together with the following two intervals (up to  $400 \text{ km s}^{-1}$ ), contains the high majority of the HSS events in SC24 (about 98%). Only 10 HSSs registered an SW speed gradient higher than  $400 \text{ km s}^{-1}$  (see also Table 3).

Table 4 shows the number of HSSs during each phase of SC24. We have also analyzed the HSS activity level during different phases of the 11-year solar cycle in some previous works (Maris and Maris, 2005, 2010, 2011). We have chosen the phase limits using the smoothed sunspot relative number, SSN, during SCs. We have considered the minimum phases as the

**Figure 10** Example of a non-geoeffective HSS. The vertical bars mark its start and its end. The dotted vertical line marks the smallest Dst value during this HSS.



intervals with  $SSN < 20$ . Practically speaking, the minimum phase between two SCs has two branches, one for each of the neighboring cycles.

The maximum phase is generally defined as the period when the relative sunspot number is higher than 80% of the cycle amplitude. This empirical definition is applied for cycles whose representation using the relative sunspot number has a simple aspect, with an increase towards the maximum and a decrease towards the minimum. In the case where the maximum phase has a two-peak shape, an interval where the relative sunspot number is larger or equal to the relative “minimum” between the two maxima of the cycle must be chosen. The ascending and descending phases of the cycles under consideration are those intervals found between the minimum and the maximum phases. Applying these definitions, SC24 phases are given in Table 4.

SC24 seems to show lower numbers of HSSs compared to the previous ones. However, computing the mean rate of HSSs/month for the entire cycle, we find that SC24 has a higher mean monthly rate compared to SC23 (Maris and Maris, 2012). Nevertheless, we note that SC23 lasted for 13 years, while SC24 comprised only 11 years.

Even these simple HSS statistics, based on the number of events and some HSS parameters, prove that the extreme levels of these phenomena, which are significant for their impact on the near-terrestrial space, do not coincide with the ones based on the sunspot relative number, which define the 11-year solar cycle.

## 5. Event Analysis

In this article, we include two examples of HSSs, a non-geoeffective one and a stream followed by a GS. These are examples that we intend to use in our future research concerning the behavior of the streams. For the description of the HSSs, we select six parameters or combinations of parameters to be shown, the same for the two Figures 10 and 11. The data resolution for all parameters shown in these figures is one hour.

**Figure 11** Example of a geoeffective HSS. As in Figure 10, the vertical dotted line shows the time when the minimum Dst value was reached.

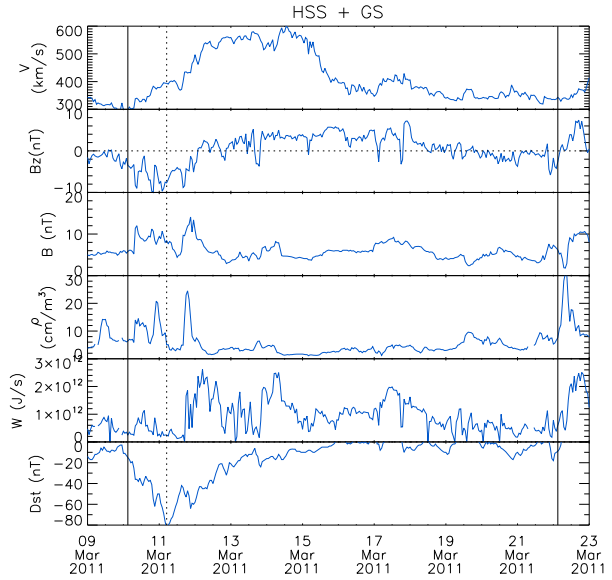


**Figure 12** SOHO/EIT 195 Å illustrating the coronal hole source for 20 and 21 November 2009. ©spaceweather.com.

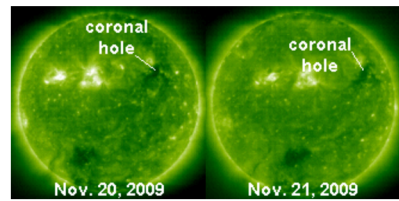


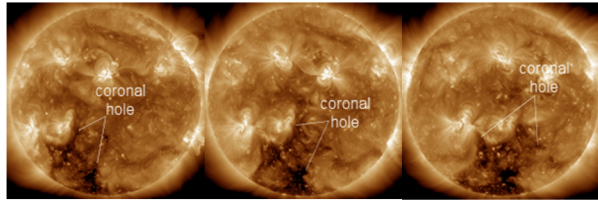
Figure 10 shows an HSS that was not associated with a geomagnetic storm. In the first row, the SW plasma speed during the stream is plotted, illustrating its increase. The second row shows  $B_z$ . The third row shows the scalar values for the interplanetary magnetic field,  $B$ . The SW plasma density is plotted on the fourth row, increasing just a bit before the speed, in agreement with a CH generated stream behavior. The fifth row shows the energy input into the magnetosphere, computed using Equation 3, with an increased contribution concomitant with the small decrease in the Dst index plotted on the last row. The drop in the Dst value is about 20 nT, but its minimum value is only  $-10$  nT. Thus, although its temporal profile would suggest a GS behavior, the values do not comply with the definitions used for GSs ( $Dst \leq -30$  nT). In this figure,  $W$  is computed at each time; that is, one value per hour.

Figure 11 shows an HSS associated with a geomagnetic storm with the same parameters shown in Figure 10. Thus, Figure 11 shows a longer-lasting increase in SW speed and three different spikes in the SW plasma density before the speed enhancement. The highest amount of energy, computed using Equation 3, was input into the magnetosphere during the recovery phase of the GS.

The main phase of the GS has two steps, probably caused by the rotations of the southern component of the IMF (see the second row in Figure 11). The recovery phase has one more Dst minima before returning to pre-storm values.

Figures 12 and 13 show the sources for the November 2009 and March 2011 streams. The source of the November 2009 HSS is a small well defined CH in the north-west quadrant of the Sun with a simple structure (Figure 12), while the source of the March 2011 HSS

**Figure 13** SDO/AIA 193 Å illustrating the coronal hole source for 9, 10, and 11 March 2011. ©spaceweather.com.



is a southern CH with a complex structure (Figure 13). This difference in source structures could be at the origin of the association with a geomagnetic storm of the second HSS, as the current flow changes with Sun's rotation.

Another difference between these two HSSs is based on the temporal evolution of  $B_z$ . In the case of the 2009 event,  $B_z$  is close to 0 with small negative values for short periods of time. For the March 2011 HSS,  $B_z$  has a longer period of negative values at the beginning of the stream and a few hours after the minimum Dst is reached.

In the case of the November 2009 HSS, the temporal profile of the energy input does not offer a good motivation for enhancing the ring current enough to justify the Dst decrease. For the March 2011 HSS, the total amount of energy deposited during the main phase of the geomagnetic storm is  $3.77 \times 10^{16}$  J for  $\Delta W_e$  and  $1.46 \times 10^{18}$  J for  $\Delta W$ , respectively, using Equations 4.

## 6. Summary

We present a detailed description of the HSS catalogue that was issued for SC24, available online at <http://www.geodin.ro/varsiti/>. The catalogue lists the characteristics for only those streams that were emitted by coronal holes. The catalogue contains 385 streams. There are 178 HSSs associated with 282 geomagnetic storms, consequently, there are 207 non-geoeffective HSSs. To the best of our knowledge, this is the only online catalogue available that includes the association with geomagnetic storms and related physical characteristics.

This catalogue encompasses the events of the entire SC24, while the catalogue by Gerontidou, Mavromichalaki, and Daglis (2018) stops in 2016, and the one by Grandin, Aikio, and Kozlovsky (2019) includes events only until 2017.

While analyzing this catalogue, we discuss a few statistical features in Section 4. We shown that the minimum phases of the 11-year solar cycles are not quiet intervals. Instead, they are periods with significant activity in the solar corona where more coronal holes with equatorial extensions can appear and become the sources of more energetic HSSs.

A comparison between our catalogue and the catalogue provided by Grandin, Aikio, and Kozlovsky (2019) clearly shows the differences in HSS detection because of the definition used.

We reiterate the remark by Maris and Maris (2012) that there is a higher probability of HSSs affecting the terrestrial magnetosphere and technological systems during the descending phase of the solar cycle. Their study, however, focused on SC23, while ours is dedicated to SC24.

We intend to continue updating the catalogue for the new solar cycle, SC25, and to make it available online as well.

**Acknowledgments** This work has been supported by a VarSITI Grant from 2017. We thank Daniela Lacatus and Alin Paraschiv for their help with programming and running issues. We also thank Ovidiu Mariş for



making this software available to our team. We acknowledge the use of OMNI data that was obtained from the GSF/SPDF OMNIWeb interface at <https://omniweb.gsfc.nasa.gov>. We also acknowledge the use of SYM-H data that was retrieved from <http://wdc.kugi.kyoto-u.ac.jp/aeasy/index.html>.

**Materials Availability** The Catalogue of High Speed Streams Associated with Geomagnetic Storms during Solar Cycle 24 is available online at: <http://www.geodin.ro/varstit/>.

## Declarations

**Conflict of Interest** The authors have no conflicts of interest to declare that are relevant to the content of this article.

## References

- Akasofu, S.I.: 1981, Energy coupling between the solar wind and the magnetosphere. *Space Sci. Rev.* **28**, 121.
- Cerrato, Y., Saiz, E., Cid, C.: 2012, *Terrestrial Magnetosphere*, 177. [ADS](#).
- Cid, C., Saiz, E., Cerrato, Y.: 2012, *Geomagnetic Storms and Substorms*, 207. [ADS](#).
- Domingo, V., Fleck, B., Poland, A.I.: 1995, The SOHO mission: an overview. *Solar Phys.* **162**, 1. [DOI](#). [ADS](#).
- Gerontidou, M., Mavromichalaki, H., Daglis, T.: 2018, High-speed solar wind streams and geomagnetic storms during Solar Cycle 24. *Solar Phys.* **293**, 131. [DOI](#). [ADS](#).
- Gonzalez, W.D., Joselyn, J.A., Kamide, Y., Kroehl, H.W., Rostoker, G., Tsurutani, B.T., Vasyliunas, V.M.: 1994, What is a geomagnetic storm? *J. Geophys. Res.* **99**, 5771. [DOI](#). [ADS](#).
- Grandin, M., Aikio, A.T., Kozlovsky, A.: 2019, Properties and geoeffectiveness of solar wind high-speed streams and stream interaction regions during Solar Cycles 23 and 24. *J. Geophys. Res.* **124**, 3871. [DOI](#). [ADS](#).
- Gupta, V., Badruddin: 2010, High-speed solar wind streams during 1996–2007: sources, statistical distribution, and plasma/field properties. *Solar Phys.* **264**, 165. [DOI](#). [ADS](#).
- Joselyn, J.A., Tsurutani, B.T.: 1990, Geomagnetic sudden impulses and storm sudden commencements: a note on terminology. *Eos Trans.* **71**, 1808. [DOI](#). [ADS](#).
- King, J.H., Papitashvili, N.E.: 2005, Solar wind spatial scales in and comparisons of hourly Wind and ACE plasma and magnetic field data. *J. Geophys. Res.* **110**, A02104. [DOI](#). [ADS](#).
- Kuklin, G.V.: 1976, Cyclical and secular variations of solar activity. *Symp. Int. Astron. Union* **71**, 147. [DOI](#).
- Lindblad, A., Lundstedt, H.: 1981, A catalogue of high speed plasma streams in the solar wind. *Solar Phys.* **74**, 197. [DOI](#). [ADS](#).
- Lindblad, B.A., Lundstedt, H.: 1983, A catalogue of high-speed plasma streams in the solar wind 1975–78. *Solar Phys.* **88**, 377. [DOI](#). [ADS](#).
- Lindblad, B.A., Lundstedt, H., Larsson, B.: 1989, A third catalogue of high-speed plasma streams in the solar wind – data for 1978–1982. *Solar Phys.* **120**, 145. [DOI](#). [ADS](#).
- Maris, G., Maris, O.: 2010, Rapid solar wind and geomagnetic variability during the ascendant phases of the 11-yr solar cycles. In: Kosovichev, A.G., Andrei, A.H., Rozelot, J.-P. (eds.) *Solar and Stellar Variability: Impact on Earth and Planets* **264**, 359. [DOI](#). [ADS](#).
- Maris, G., Maris, O.: 2011, Fast solar wind and geomagnetic variability during the descendant phase of the 11-yr solar cycle. In: Zhelyazkov, I., Mishonov, T. (eds.) *Amer. Inst. Physics C.S.* **1356**, 177. [DOI](#). [ADS](#).
- Maris, G., Maris, O.: 2012, In: Maris, G., Demetrescu, C. (eds.) *High Speed Streams in the Solar Wind During the 23rd Solar Cycle*, Research Signpost Publ., Trivandrum, 97.
- Maris, O., Maris, G.: 2005, Specific features of the high-speed plasma stream cycles. *Adv. Space Res.* **35**, 2129. [DOI](#). [ADS](#).
- Mavromichalaki, H., Vassilaki, A.: 1998, Fast plasma streams recorded near the Earth during 1985–1996. *Solar Phys.* **183**, 181. [DOI](#). [ADS](#).
- Mavromichalaki, H., Vassilaki, A., Marmatsouri, E.: 1988, A catalogue of high-speed solar-wind streams: further evidence of their relationship to  $A_p$ -index. *Solar Phys.* **115**, 345. [DOI](#). [ADS](#).
- Muntean, G.M., Besliu-Ionescu, D., Dobrica, V.: 2018, Complex catalogue of high speed streams and geomagnetic storms during Solar Cycle 24 (2009–2016). In: *VarSITI Newsletter* **17**, 5.
- Pesnell, W.D., Thompson, B.J., Chamberlin, P.C.: 2012, The Solar Dynamics Observatory (SDO). *Solar Phys.* **275**, 3. [DOI](#). [ADS](#).
- Phillips, J.L., Bame, S.J., Barnes, A., Barraclough, B.L., Feldman, W.C., Goldstein, B.E., Gosling, J.T., Hoogeveen, G.W., McComas, D.J., Neugebauer, M., Suess, S.T.: 1995, Ulysses solar wind plasma observations from pole to pole. *Geophys. Res. Lett.* **22**, 3301. [DOI](#). [ADS](#).

- Sykora, J.: 1992, The green corona, the solar wind and geoactivity. *Solar Phys.* **140**, 379. DOI. ADS.
- Wang, C., Han, J.P., Li, H., Peng, Z., Richardson, J.D.: 2014, Solar wind-magnetosphere energy coupling function fitting: results from a global MHD simulation. *J. Geophys. Res.* **119**, 6199. DOI. ADS.
- Wanliss, J.A., Showalter, K.M.: 2006, High-resolution global storm index: Dst versus SYM-H. *J. Geophys. Res.* **111**, A02202. DOI. ADS.
- Zhang, J., Richardson, I.G., Webb, D.F., Gopalswamy, N., Huttunen, E., Kasper, J.C., Nitta, N.V., Poomvises, W., Thompson, B.J., Wu, C.-C., Yashiro, S., Zhukov, A.N.: 2007, Solar and interplanetary sources of major geomagnetic storms ( $Dst \leq -100$  nT) during 1996–2005. *J. Geophys. Res.* **112**, A10102. DOI. ADS.

**Publisher's Note** Springer Nature remains neutral with regard to jurisdictional claims in published maps and institutional affiliations.